De-icing of propeller blades: electro-thermal vs elctro-mechanical techniques effieciency comparison

J. Kanfoud, S. Soua, T-H. Gan
TWI Ltd, Integrity Management Group
Cambridge, Cambridgeshire, CB21 6AL, United Kingdom
Telephone: +44(0)1223899000
Telfax: +44(0)1223892588
email: jamil.kanfoud@twi.co.uk

Abstract

Research on de-icing started at the dawn of the 20th century as aeronautic industry grew aware of the risks created by the accumulation of ice on the airplane structure in general and the aerodynamic surfaces in particular. Nowadays, the anti-icing systems are an integral part of the design of the aerodynamic surfaces (blades in helicopters and propellers, wings and stabilisers) and ensure safety in all weather conditions.

The techniques most commonly used by the aeronautic industry are the electro-thermal, pneumatic de-icing boots and hot air from engines. All these techniques have shown their limitation with regards to reliability, energy efficiency and impact on aerofoil design. The demand for low power ice protection systems will stretch current technologies and the analytical tools required to support them. In this paper, we propose to compare an electro-mechanical de-icing technique and electo-thermal de-icing technique on propellers blades. The blades offer a very challenging environment with the rotation of the blades increasing the rate of accretion and the blades requiring very lightweight technological solutions. The electro-thermal technique is based on the use of graphite heaters embedded in the blade or covering it. The electro-mechanical technique is based on the use of an impulsive vibration lasting 1ms. The vibration is created by the induced repulsive electromagnetic forces created in a set of conductors generating a shear stress able to disband the ice from the blade surface. The electro-thermal technique is well documented. In this paper, both technologies will be compared on the same design and their efficiency with regards to blade coverage, de-icing time and power efficiency. Simulations are conducted using FEA simulations and criteria defined in order to assess both technologies. Conclusions are drawn on the advantages and disadvantages of each solution.

1. Introduction

Economic pressures dictate that aircrafts must keep flying in known adverse weather conditions where ice formation on the aircraft is a flight risk and these pressures will continue to increase. In addition, there will always be risks that a flight will run into unpredictable icy forming conditions even when departing in perfect weather.

On an aircraft, the leading edges of the wings, flight surface control mechanisms and the moving components of the propulsion system, motors, propellers, fans and rotors etc are

all especially vulnerable to ice accretion in flight, as well as on the ground. The increased mass increases drag, decreases lift and especially when unevenly distributed, prejudices the flight equilibrium and especially dangerous, it lowers the minimum stall angle. Ice also causes control and propulsion mechanisms to be reduced in efficiency and even seize up to endanger the aircraft. Ice can be especially dangerous on propellers and rotors because these structures are finely balanced so that moderate ice accretion can seriously affect the balance, causing stress levels which could threaten structural integrity[1].

Ice accretion takes multiple forms[1,2]. Hoar frost takes the form of crystalline scales, needles or feathers, and is formed by sublimation of water vapour, and can arise can even in clear air ie without clouds. Rime ice is white, opaque and brittle with rough surfaces. It is formed on cold surfaces by passage through clouds at temperatures below -10°C with small and supercooled water droplets freezing rapidly resulting in entrapped air bubbles. Clear ice is formed on a cold surface passing through clouds at temperatures between -10°C and 0°C when supercooled water droplets spread out before freezing slowly.

Severe icing ie an accretion rate of > 12gcm-2/hour usually compels a crew to change flight path (direction or altitude) immediately[2]. Flight accidents attributable to icing are more common in smaller aircrafts including commuter planes and particularly open rotor aircraft, which fly for most of the time at icing altitudes. In the USA alone, over the past 30 years, approximately 40 deaths a year arise in an average of 30 ice related accidents a year mostly in the winter months.

Due to the importance of ice in flight safety, there are regulations for airports and airlines that operate during icing conditions. The International Civil Aviation Documents (ICAO) documents particularly Annex 6 operation of Aircraft give de-icing requirements and guidelines and so does the Manual of Aircraft Ground De-icing/Anti-icing Operations.

Many Ice Protection Systems (IPS) exist in the market. The current techniques used are de-icing fluids (glycol based), pneumatic systems, electrothermal systems and hot air bleed systems. To a lesser extent, a weeping wing technology using glycol is used as well. Most of these techniques show limitations either in efficiency, reliability or high power requirements.

TWI is working on evaluating alternative technologies for low power effective de-icing technologies for use on blades under a European CleanSky collaborative project ICEPS-ORPS[3] with SNECMA. Two technologies are evaluated during this project, classic electrothermal systems based on the use of graphite with extremely high heat conductivity coefficient and impulsive vibration system using electromagnetic induced vibration.

2. Electrothermal heating modelling

2.1 Introduction

Electro-thermal systems use resistive circuits buried in the airframe structure to generate heat when a current is applied. Three configurations are possible:

- De-icing systems: periodically shed small ice build-ups by melting surface-ice interface with a high rate of heat input. When the adhesion at the interface becomes zero, the aerodynamic forces (wings stabilizers) and/or the centrifugal forces (propeller blades) remove the ice
- Anti-icing systems: These systems prevent the ice from building up. There are two categories of anti-icing systems
    - Running-wet anti-icing systems: provide only enough heat (typicallyT_Surface≥5°C) to prevent freezing on the heated surface. Beyond the heated surface of a running-wet system, the water can freeze resulting in runback ice. Running-wet systems must be designed carefully so as not to permit build-up for runback ice in critical locations.
    - Evaporative anti-icing systems: supply sufficient heat (typicallyT_Surface≥20°C) to evaporate all water droplets impinging upon the heated surface.

Anti-icing requires more power than de-icing. Hence, anti-icing systems are capable of achieving de-icing as well with less energy consumption. Different manufacturers have worked on developing anti-icing and de-icing systems by improving the materials and the layout of the systems developed in the 1st half of the 20th century.

ThermaWing^{TM} and Spraymat^{TM} are examples of technologies using electrothermal elements for either de-icing or anti-icing. The ThermaWing is a heating layer attached to the leading edge of aerodynamic elements of small planes. Sprymat is a more complex technology using sprayed metals embedded inside aerofoils. It has been used on helicopter blades and on the 787 dreamliner wings among other applications.

2.2 Modelling

The modelling of electrothermal deicing requires the modelling of all phenomena taking place. The surface of the blade is bombarded with supercooled water droplets (-30°C, 40kPa). The de-icing system provides power to counterbalance the heat energy loss. The phenomena contributing to the loss of energy are the convective cooling, the fusion cooling and the evaporative cooling. In the case of running wet de-icing, the melting of ice leads to loss of energy corresponding to the latent heat of fusion. In the case of evaporative anti-icing, both melting and evaporation occurs. The latter is due to the evaporation of water and depends on the air humidity, the blade surface temperature and the saturation pressure. Latent heat of vaporisation is much more important than the latent heat of fusion generally and for water in particular requiring more power from the anti-icing system.

The phenomena helping de-icing are the aerodynamic heating due to the friction in the boundary layer over the surface and the kinetic heating due to the impinging accelerated supercooled droplets.

Meier and Al[4] propose the pre-sizing of electrothermal de-icing without taking into account the geometry of the aerofoils but with the inclusion of all phenomena described above. In this paper, only the main phenomena are taking into account; conduction and convection and the electrothermal heat source. The geometry of the blades defined by the end user.

2.2.1 Heat conduction

Heat conduction is the transfer of internal energy by microscopic diffusion and collision of particles within a body due to a temperature gradient. The heat conduction is given function of the temperature T by the following differential equation:

$$k\Delta T + \dot{Q} = \rho C_p \frac{\partial T}{\partial t} \quad (1)$$

Where $\dot{Q}$ corresponds to the rate of energy generation per unit volume inside the control volume; heat might be generated by a chemical reaction for example. The right side term corresponds to the rate of increase of internal energy. The parameters of the equations are:

- $\boldsymbol{k}$ Thermal conductivity (W/m/°K)
- $\boldsymbol{C_p}$ Specific heat (J/Kg/°K)
- $\boldsymbol{\rho}$ mass density (Kg/m3)

2.2.2 Heat convection

Convective heat transfer is often referred to simply as convection. It is the transfer of heat from one place to another by the movement of fluids. The equation governing the convective heat transfer is known as Newton's law of cooling and is given by:

$$\frac{\partial Q}{\partial t} = hA(T_S - T_\infty) \quad (2)$$

Where:

- **Q** is the thermal energy gained or dissipated by convection
- **h** is the convective heat transfer coefficient (W/m2/°K)
- $\mathbf{T_S}$ is the temperature of the surface of the solid
- $\mathbf{T_\infty}$ is the temperature of the environment, far from the solid surface

The difficulty with convection heating consists in determining the convective heat transfer coefficient. It depends on many parameters: the geometry (planar, circular, etc), the speed of the airflow on the surface (238m/s) and the convection regime (laminar, turbulent). The turbulence regime considerably influences the convection coefficient with the convection decreasing from the leading edge of a plate until it reaches the transition layer where it increases steeply. It once again decreases along the turbulent layer but the convection coefficient values remain high compared to the laminar layer.

The blade geometry used for this study is shown Figure 1. The cross section at the root is shown in Figure 2. As show below, the geometry of the blade has been kept simple on purpose by the end user

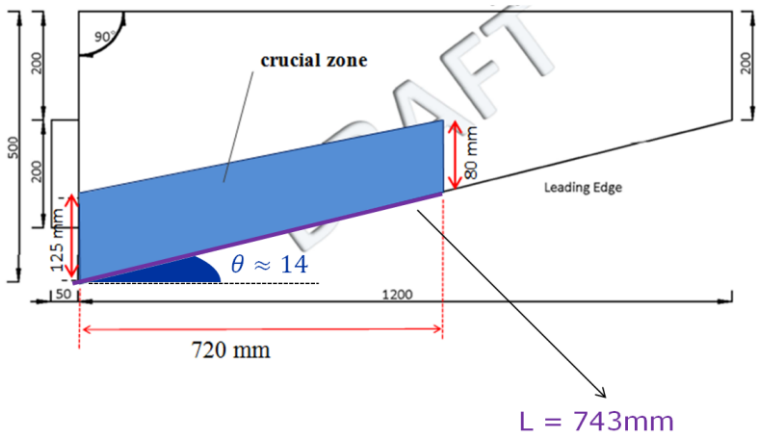

Figure 1. Blade geometry (area where de-icing is applied highlighted in blue

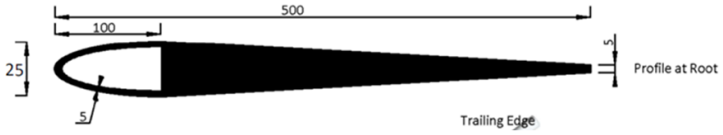

Figure 2. Cross section of the blade

For the blade used, two areas are identified for computing the convection coefficient:

- The leading edge: it corresponds to the area starting at the stagnation point and covering an angle of 80° either side. The leading edge convection coefficient is calculated assuming a cylindrical shape.
- The area aft of the leading edge: even though this area is not perfectly planar, the convection coefficient will be calculated assuming a planar area.

- *Convection coefficient for the planar area*

The convection coefficient can be computed locally or averaged on the length of the plate L. For this project, the plate maximum length is 0,125m. The convective heat transfer coefficient is given by:

$$h = k\frac{Nu_L}{L} \tag{3}$$

Nu_L is the averaged Nusselt number which is the ratio of convective to conductive heat transfer. When Nu≈1, the flow is laminar. When Nu≥100, the flow is turbulent. The Nusselt number is a function of the Reynolds number and Prandtl number.
Reynolds number helps predict flow patterns. It distinguishes between regimes of fluid flow (laminar, turbulent). It is defined as the ratio of inertial forces to viscous forces and is given for a planar surface by:

$$Re = \frac{\rho . U_{\infty} . L}{\mu} \tag{4}$$

Where:

- U_{∞} is the relative speed of the wind to the blade surface U_{∞}=238m/s
- μ is the dynamic viscosity. For the air at T=-30°C, μ =15,88 10-6 Ns/m2
- L=0,125m

Finally we have a Reynolds number corresponding to a turbulent regime:

$$Re \approx 269000 \tag{5}$$

The Prandtl number, contrarily to the Reynolds number is a characteristic of the material. It is the ratio between momentum diffusivity and thermal diffusivity. Prandtl control the relative thickness of the heat and momentum (velocity) layers. When Pr is small, heat diffuses very quickly (by conduction) compared to momentum (by convection).

The Prandtl number is Pr=0,721. The formula for the average Nusselt number of a planar surface corresponding to a turbulent flow ($Re > 5.10^5$ et $Pr > 0{,}5$) is given[5] by

$$Nu_L = 0.036\, Pr^{0.33} \left[{Re_L}^{0.8} - 23200 \right] = 3750{,}36 \tag{6}$$

Finally, we obtain the convective heat transfer coefficient for the planar part:

$$h_L = k \frac{Nu_L}{L} = 658{,}86 \mathrm{W/m^2/K} \tag{7}$$

- *Convection coefficient for the cylindrical area*

For planar structures, the computation of the convective heat coefficient requires the evaluation of the Nusselt number. For cylindrical structures, the same applies:

$$h_D = k \frac{Nu_D}{D} \tag{8}$$

The difference is that the Nusselt number requires computing the Reynolds number. For cylindrical structures, empirical formulae are used to evaluate the Nusselt number.
Martinelli & co[5] developed and verified an empirical formula to calculate simply the convective heat transfer coefficient over wings. It evaluates the local Nusselt number over cylindrical shape. The angle θ is the angle from the stagnation point (θ=0 corresponds to the stagnation point). The formula is valid for angles ranging between 0° and 80°.

$$Nu_{\theta} = 1{,}14 \sqrt{\frac{\rho U_{\infty} D}{\mu}}\, Pr^{0.4} \left[1 - \left(\frac{\theta}{90} \right)^3 \right] \tag{9}$$

In order to calculate an average Nusselt number between 2 angles θ_1 andθ_2, the above formula is integrated.

$$Nu_D(\theta_1 \to \theta_2) = \frac{1}{\theta_2 - \theta_1} \int_{\theta=\theta_1}^{\theta_2} Nu_\theta \, d\theta = \frac{1.14}{\theta_2 - \theta_1} \sqrt{\frac{\rho U_\infty D}{\mu}} \, Pr^{0.4} \left[\theta - \frac{1}{4}\frac{\theta^4}{90^3}\right]_{\theta_2} \quad (10)$$

The average Nusselt number on the leading edge is:

$$Nu_D(0 \to 80) = 363{,}1 \quad (11)$$

The convective heat transfer coefficient is:

$$h_D(0 \to 80) = 886 \ \mathrm{W/m^2/K} \quad (12)$$

Table 1 gives an evaluation of the Nusselt number and convective heat transfer coefficient between different angles:

Table 1. Nusselt and convection coefficient averaged between different angles

Angle Covered (°)	Nusselt Number	Convection coefficient (W/m2/K)
0-20	439.23	1071.71
20-40	422.31	1030.44
40-60	361.89	883.02
60-80	228.98	558.71

2.3 Simulations

During this project, many materials have been assessed to evaluate if they can be used for the electrothermal heating. The material selected is graphite as it can ensure both functionalities: electrical resistance and efficient heat conductor. Actually graphite is the material with best heat conductivity (1500W/m/K) after diamond. eGraph develops very low thicknesses graphite layers (0,17mm) which is important as it means that this element will have little weight compared to other de-icing solutions, a very important parameter when it comes to de-icing.

For the modelling, three layers are considered, the blade material, then the graphite heating element and finally the ice layer. The thickness of the ice was modelled with 2mm and 4mm. The properties of the materials in the modelling are given by Table 2.

Table 2 Properties of the materials in modelling

Properties	Blade	Ice	Graphite SS1500
K (W/m/°K)	1.64	2.18	1500
C_p (J/Kg/°K)	1019.5	2108	830
Rho (Kg/m^3)	1575	917	2250

The modelling has been carried out in 2D. There is only one boundary condition outside the blade which is forced convection (Figure 2). The convection coefficient is defined by area with the values calculated separately for the circular shape leading edge

(886W/m^2/K) and the planar area (659W/m^2/K) of the blade. Through the thickness of the blade, the different layers (ice, graphite, blade) have a temperature continuity condition. This means that there is no heat transfer in the cavity inside the blade.

De-icing is achieved when the wing surface temperature exceeds 0°C. The simulation results (Figure 3) show that:

- 10kW/m^2 allows de-icing only for 4mm thickness ice or higher but take more than 40s to achieve that which is beyond the maximum time required in the specifications
- 12kW/m^2 allows de-icing only for 4mm ice thicknesses with a time of 26s
- 14kW/m^2 allows de-icing both for 2mm and 4mm ice-thickness within 20s

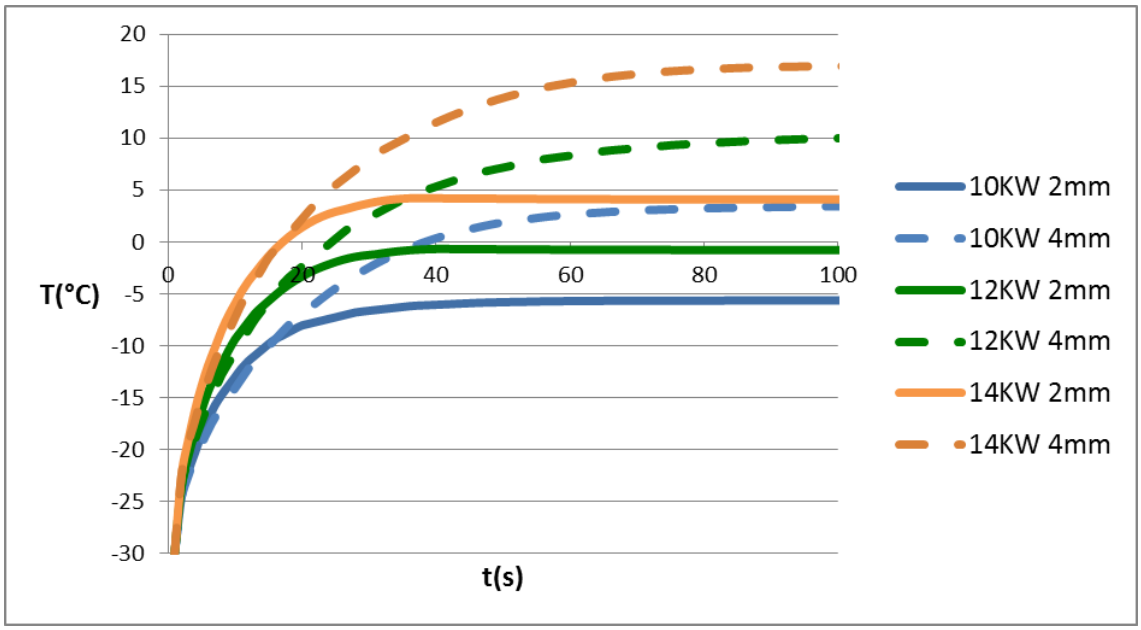

Figure 3 Electrothermal de-icing of the blade with 2mm and 4mm ice layers

The area where de-icing is to be applied to the blade is approximately 0,15 m2. Hence, the power necessary to de-ice a blade is:

$$P_{blade} = 2,1\ kW/blade \tag{13}$$

Depending on the length of the de-icing cycle (60s, 120s, etc), we can determine the power necessary to achieve de-icing in a cycle. 5kW power supply insures de-icing of two blades at a time, 10kW four blades, etc.

3. Electromagnetic induced transient vibrations

3.1 Introduction

Many techniques exist using electromagnetic induced vibrations for de-icing. Very few are very successful industrially. Among these techniques, there is the sonic pulse electro-expulsive deicer (U.S. Patent 6,102,333) using coil actuators applying force to the outer skins of aerofoils. The electro-expulsive separation system is a hybrid system using rubber boots but instead of using air to inflate them, current passes through conductors generating an electromagnetic field which generates a mechanical force to knock the ice off the flight surface.

The technologies mentioned above are applicable to wings but are too bulky for blades. Hence the best solution consists in using conductive strips fabricated on a flexible di-electric sheet. A current induced electromagnetic field is created by two superposed strips at least; the current leads to the acceleration of the strips which results in a very important transient acceleration of the surface of the blade. The force created for a microsecond results in shedding off the ice from the blade surface. To achieve this target, the blade is covered by a flexible rigid metallic layer. The flexible rigid metallic layer could be at the same time the erosion shield of the blade.

3.2 Modelling

This technique relies on the use of an electromagnetic field to generate an impulsive mechanical force to de-ice. In order to solve this problem using modelling, the mechanical force necessary to disband the ice from the blade is determined first. Then the size of the actuators and the electrical power necessary to create the electromagnetic force are estimated.

3.2.1 Mechanical modelling

The objective of this section is to determine the mechanical force necessary to de-ice the critical area of the blade (Figure 1 in blue). The de-icing criteria has been given by the end user and it states that the shear stress in the interface between the blade and the ice must exceed a threshold:

$$\tau \geq 0{,}4MPa \tag{14}$$

In order to achieve this, a transient mechanical force is applied for one millisecond. The force is given by:

$$f(t) = \frac{A}{2}\sin(2\pi.500.t) \tag{15}$$

The geometry of the blade modelled using COMSOL Multiphysics is given by SNECMA. There is a 1mm thick metallic layer and covered with a 2mm-thick layer of ice. The metallic layer has been simulated as aluminium. The characteristics of the materials are given by Table 3.

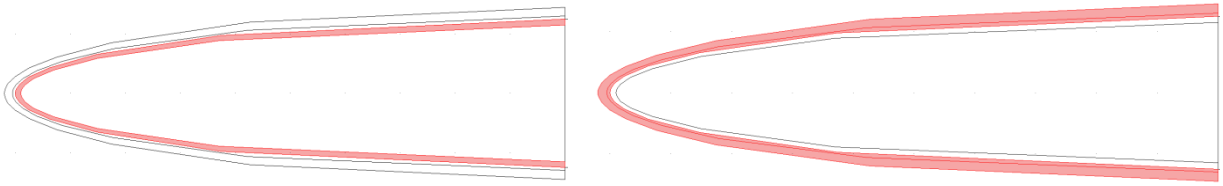

1mm thick rigid flexible layer 2mm thick ice layer

Figure 4. Design of the front of the blade used for simulations

Table 3. Materials mechanical characteristics

	E (MPa)	ν	$\rho(Kg/m^3)$
Ice	8,3	0,351	917
Aluminum	70	0,33	2700
Epoxy/HS Carbon Fiber	46,2	0,337	1575

In 2D, the stress tensor is given by:

$$[\sigma]_{2D} = \begin{bmatrix} \sigma_{xx} & \sigma_{xy} \\ \sigma_{xy} & \sigma_{yy} \end{bmatrix}$$

The blade cross section is in the $(\vec{x}, \vec{y})$ plane. The normal to the interface between the metallic layer and the ice layer is in the same plane. Hence, it can be written as follows:

$$\vec{n} = \begin{bmatrix} \cos\theta \\ \sin\theta \end{bmatrix}$$

The stress vector is given by:

$$\vec{t} = [\sigma].\vec{n} = \begin{bmatrix} \sigma_{xx}\cos\theta + \sigma_{xy}\sin\theta \\ \sigma_{xy}\cos\theta + \sigma_{yy}\sin\theta \end{bmatrix}$$

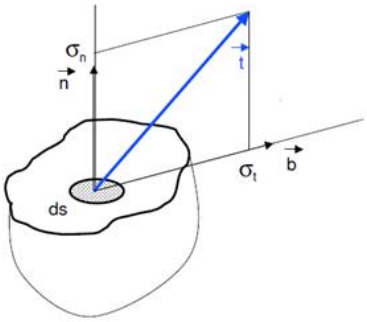

Figure 5. Shear stress definition

As shown in Figure 5, there are two components in the shear stress vector, the normal component σ_n corresponding to extension-compression stress and the tangent component σ_t corresponding to the shear stress. The shear stress component is $\overrightarrow{\sigma_t} = \vec{n} \wedge \vec{t}$

The shear stress σ_t is finally given by:

$$\sigma_t = \frac{1}{2}(\sigma_{yy} - \sigma_{xx})\ sin\ 2\theta + \sigma_{xy} \cos 2\theta \tag{16}$$

In order to evaluate the effect of the application point of the force, three positions will be evaluated for shear stress which are shown in Figure 6 as a 2D plot does indicate the same precision.

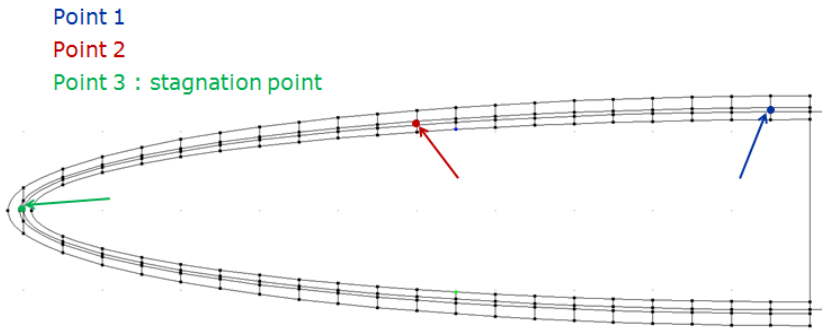

Figure 6. Points where the shear stress is evaluated

Simulations were conducted to determine the optimum application point of the electromagnetic transient force. Once the position has been determined, the optimum amplitude of the force has to be determined as well to give best de-icing with the minimum energy.

The shear stress is observed in the figures below at t=0,5ms which corresponds to the time when the transient force reaches its maximum value. Whenever $\tau \geq 0{,}4$MPa the shear stress is in a white colour.

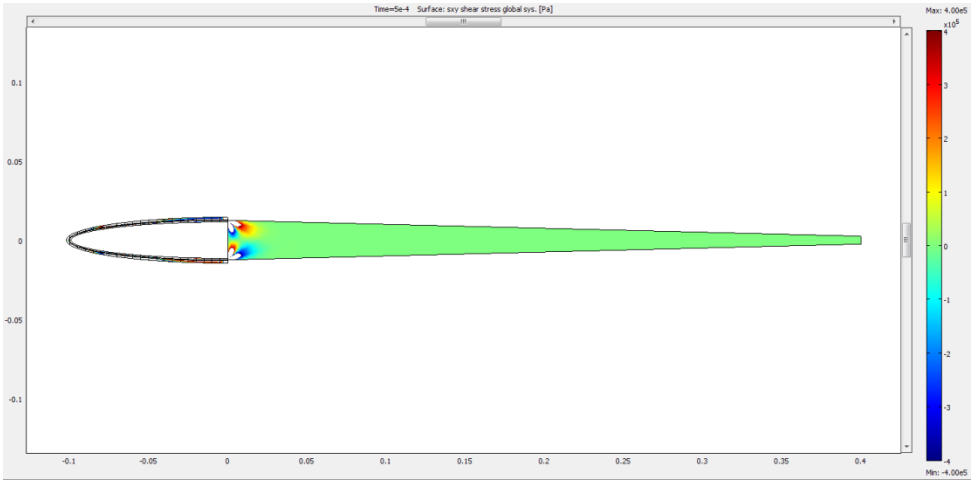

Figure 7. Shear stress with a 3kN force

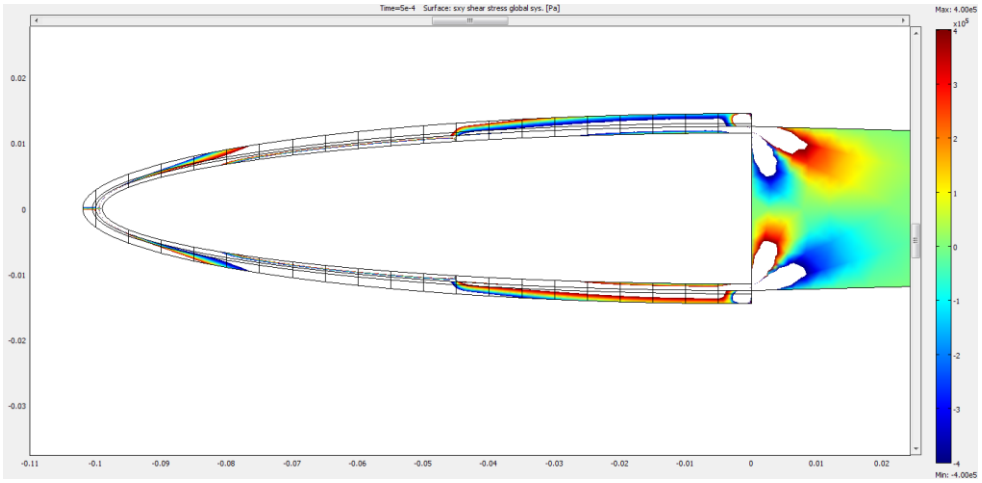

Figure 8. Shear stress with a 3kN force (Zoom)

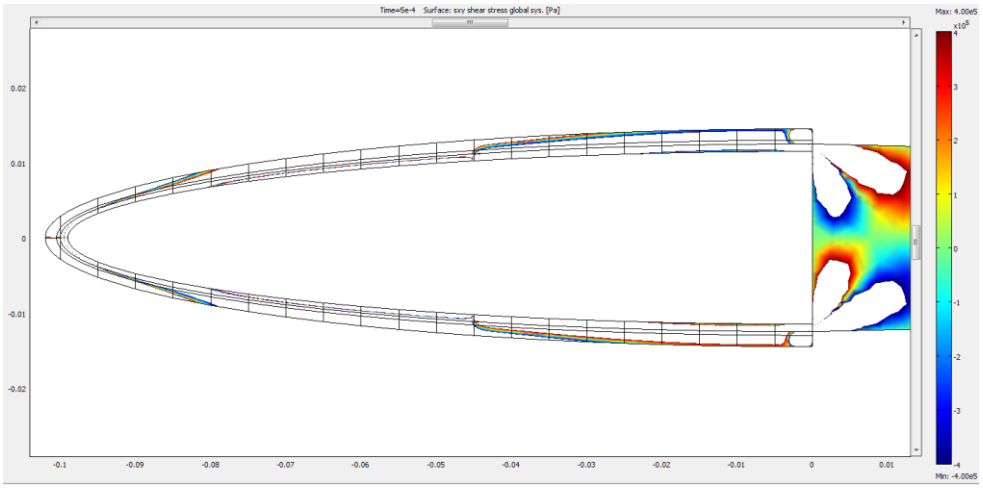

Figure 9. Shear stress with a 6kN force (Zoom)

The figures above show the shear stress for different values of the electromagnetic transient force. The stress values on the area where de-icing is applied shows that the threshold shear stress is exceeded on most of the interface between the blade and the ice (white areas) even with a force as low as 3kN.

The figures lack precision though. Hence, the shear stress will be evaluated in three points of the interface between the blade and the ice (Figure 6). The results are given by the three figures below:

- Figure 10 shows the shear stress at Point 1 for different forces amplitudes
- Figure 11 shows the shear stress at Point 2 for different forces amplitudes
- Figure 12 shows the shear stress at Stagnation Point 3 for different forces amplitudes

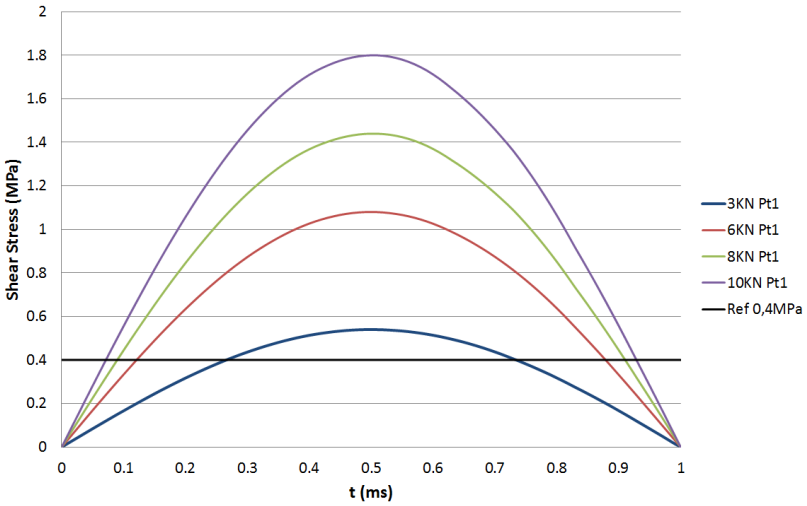

Figure 10. Shear stress at Point 1 for different force amplitudes

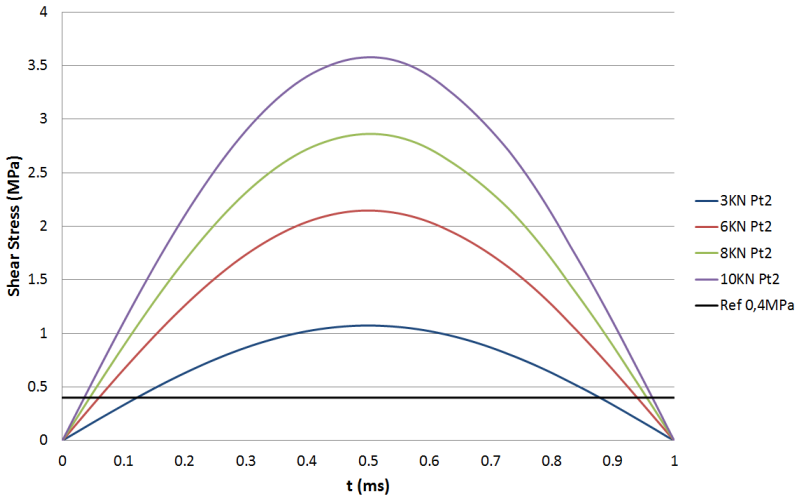

Figure 11. Shear stress at Point 2 for different force amplitudes

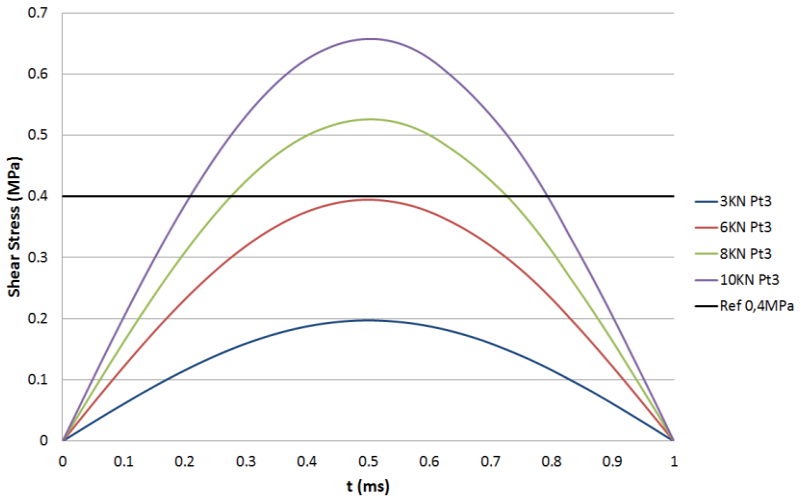

Figure 12. Shear stress at stagnation point 3 for different force amplitudes

For points 1 (Figure 10) and 2 (Figure 11), the shear stress threshold is exceeded with either force. For the stagnation point 3 (Figure 12), a force greater than 6kN is necessary to achieve de-icing.

The force amplitude is chosen is **A=8kN**, hence:

$$f(t) = \frac{A}{2} sin(2\pi.500.t) \quad with\ A = 8kN$$

2.2.2 Sizing of the actuators

The actuators designed to create the impulsive electromagnetic force are simple copper conductor strips with a dielectric separation. Each actuator is made of two strips where opposing currents create repulsive electromagnetic fields. The strip linked to the metallic layer is accelerated for 1ms in order to disbond ice.

In the previous section, it is shown that the force necessary to disbond the ice is:

$$f(t) = \frac{A}{2} sin(2\pi.500.t) \quad with\ A = 8kN$$

The sizing of the actuators is done using the following formula[6]:

$$f(N/m) = 4.10^{7} I_1 I_2 \left\{ b.tan\left(\frac{b}{d}\right)^{-1} - \frac{d}{2} ln \frac{d^2 + b^2}{d^2} \right\} \quad (17)$$

Where:

- b is the conductor width
- d is the conductors separation
- I_1 is the current in one conductor strip
- I_2 is the current is in the other conductor strip

To simplify the sizing, the current in both strips is considered equal and the dimensions of the conductors are fixed:

- $I=I_1= I_2$
- b=10mm
- d=0,5mm

The current necessary to achieve de-icing is:
$I_1= I_2 \approx$ 11340 A
Given that the blade has to be de-iced on both the top and bottom sides, the current necessary to achieve de-icing is:
$I_1= I_2 \approx$ 22700 A
Given that each blade requires 1ms for de-icing, we are considering applying 10 cycles to the blade with each cycle requiring a current of:
$I_1= I_2 \approx$ 2270 A

More important than the current is the power necessary to achieve de-icing. In order to compute the power, we have to determine the voltage in the conductors. The resistance of the coil conductors is:

$$R = \rho\frac{l}{A} = 0{,}25m\Omega$$

With

$$\rho = 1{,}68\ 10^{-8}\Omega m \quad A = 5mm^2 \quad l = 0.0745m$$

The voltage for 2 conductors opposite to one another for each actuator is:
$\boldsymbol{V = 2\ R.I = 0,\ 56\ V}$
The instantaneous power required to achieve de-icing is:

$$\boldsymbol{P = V.I \approx 1{,}3\ kW} \tag{18}$$

The power levels are low, particularly with times not exceeding 1ms. The energy necessary is power multiplied by time. The time necessary to de-ice the whole blades consists in the number of blades multiplied by the number of areas de-iced separately in each blade.

- Number of blades 22
- Number of areas to de-ice per blade 10
- Duration of each deicing cycle 1ms

The energy necessary for a de-icing cycle is then:

$$\boldsymbol{E = P.T \approx 285\ J} \tag{19}$$

Assuming that there is a 1ms gap between de-icing cycles and knowing that each de-icing cycle takes 1ms. There are 220 areas to de-ice in the blade of the open rotor propeller. Consequently, this technology is the one requiring the minimum time to achieve de-icing of 0,44s.

Given that the system uses energy of 285J in 0,44s, the power of the system is:

$$\boldsymbol{P_{System} \approx 650W \approx 197W/m^2} \tag{20}$$

4. Conclusions

In this paper, two de-icing techniques were modelled on the same geometry blade covered by a 2mm layer ice. The first is a classical electrothermal technique which has been optimised by the use of very high conductivity graphite heating elements. Modelling shows that for a 2mm ice layers requires 14kW/m^2 to achieve deicing in 20s.

The electromagnetic induced transient vibrations are a disruptive technology which has been applied only for stabilizers commercially. In this paper, modelling of these actuators for blades is tested. Simulations results show that this technology is very effective as it has very little power requirements of less than 0,2kW/m^2 and that it

achieves de-icing in less than a second. Henceforth, not only does this technology allow much higher efficiency with effects on fuel consumption of the planes but allows successive de-icing cycles separated by a second, which allows much more effective de-icing in severe icing conditions.

Acknowledgements

This work was developed under the project ICEPS-ORPS (Open Rotor Propellers Ice Protection System) partly funded by the EC under the CleanSky research program. Grant Agreement Number 620148. ICEPS-ORPS is a collaboration between the following organisations: SNECMA (Groupe SAFRAN) , Brunel Innovation Center and TWI LTD.

References and footnotes

1. Federal Aviation Administration, 'Aviation Weather', Snowball publishing, July 2012.
2. G. Mingione and E. Denti 'Flight in icing conditions'.
3. http://www.iceps-orps.eu
4. O. Meier, D. Scholz, 'A handbook method for the estimation of power requirements for electrical de-icing systems' DLRK, Hamburg, August 2010.
5. F. Kreith; R.M. Manglik; M.S. Bohn, 'Principle of Heat Transfer 7th Edition', CENGAGE Learning, 2011
6. L. J. Adams & Al, 'Electro-repulsive separation system for deicing', US Patent 4,875,644, October 1989